Evaluation of Special Sensor Microwave Imager/Sounder (SSMIS) Environmental Data Records

Ninghai Sun
I. M. Systems Group, Inc., Kensington, Maryland, USA
Fuzhong Weng
NOAA/National Environmental Satellite, Data and Information Service/Center for Satellite Applications and Research, Camp Springs, Maryland, USA

Abstract

Compared to the Special Sensor Microwave Imager (SSM/I), the new Special Sensor Microwave Imager/Sounder (SSMIS) aboard the Defense Microwave Satellite Program (DMSP) F16 satellite has the similar seven imaging channels except for two at 85.5 GHz replaced by the 91.655 GHz frequency. After the NRL calibration of SSMIS imager channels, the temperature data record (TDR) can be utilized operationally to derive both atmospheric and surface parameters. In this study, several products are developed from the SSM/I heritage algorithms, including total precipitable water, cloud liquid water path, snow cover, sea ice cover, rain rate and land surface temperature. Some new products are also derived from SSMIS, such as land emissivity. The retrieved products from F15 SSM/I and F16 SSMIS are inter-compared to quantify the mean bias and standard deviation. It is found that because of both the relatively small mean bias and standard deviation the F16 SSMIS products, such as total precipitable water, cloud liquid water path, snow and sea ice, may replace the SSM/I products for operational use. However, discrepancies remain in the global rainfall estimates, land surface temperature and land emissivity produced by each sensor. This is likely due to the imperfect F16 SSM/I-like channels to F15 SSM/I channels linear mapping, especially for 91.655 GHz channels, whose frequency is shifted from 85.5 GHz in SSM/I.

INTRODUCTION

The Special Sensor Microwave/Imager (SSM/I) was developed as part of the Defense Meteorological Satellite Program (DMSP) and first launched in June 1987 aboard DMSP F-8 satellite. The SSM/I measures thermal radiation from the Earth's surface and atmosphere at four frequencies from 19.35 GHz to 85.5 GHz with both vertical and horizontal polarizations, and has provided critical information on global hydrological parameters such as water vapor, cloud water and precipitation. SSM/I data and the retrieved products have been widely used in data assimilation systems with positive impacts (Tsuyuki 1997; Deblonde 1999; Hou et al. 2000; Okamoto and Derber 2006).

The DMSP F16 satellite was successfully launched on October 18, 2003, carrying the first Special Sensor Microwave Imager/Sounder (SSMIS) onboard. SSMIS marks the beginning of a new series of passive microwave conically scanning imagers and sounders to be launched over the next two decades. This instrument provides measurements at 24 channels. Seven include imaging channels, similar to SSM/I, of which two channels have been slightly shifted from the SSM/I 85.5 GHz vertical and horizontal polarizations (V and H will be used to represent vertical horizontal polarizations for simplicity hereafter) to the SSMIS 91.655 GHz V and H. SSMIS also has seven lower atmosphere temperature sounding (LAS) and six upper atmosphere temperature sounding (UAS) channels near the 50 to 60 GHz oxygen absorption

bands. In addition, SSMIS contains one horizontally polarized 150 GHz and three horizontally polarized channels with double sidebands about 183.31 GHz for mid-to-upper troposphere water vapor sounding. With a larger scan angle, 144^o versus 102^o for SSM/I, SSMIS increases the imaging channel scene number to 90 compared with 64 in the SSM/I A-scan and to 180 from 128 in the SSM/I B-scan. This effectively reduces the scan gap area in mid-latitude regions. Based on its ability to measure microwave radiation from a broader spectrum, SSMIS can provide temperature profiles up to 80 km altitude as well as water vapor profiles and surface information under varying weather conditions.

This study will focus on the evaluation of the retrieval of a number of heritage environmental parameters from F16 SSM/I-like channels, which are 19.35 GHz V/H, 22.235 GHz V, 37.0 GHz V/H, and 91.655 GHz V/H, in the SSMIS. In section 2, the F16 SSMIS data and its calibration algorithm are briefly introduced. The description of retrieval algorithms and the inter-comparison results of these environmental parameters from F15 and F16 measurements will be given in section 3. The final section will summarize the results of this study and give a preliminary conclusion based on the discussions.

DMSP Data and Evaluation Methodology

National Oceanic and Atmospheric Administration (NOAA)/National Environmental Satellite Data, Information Services (NESDIS) received SSM/I and SSMIS antenna brightness temperature data records (TDRs) through a data-sharing agreement with DMSP. The F16 SSMIS TDRs have been archived at NOAA/NESDIS since January, 2005. At present, DMSP F15 and F16 are used as primary sensors in NOAA operations with DMSP F-13 and F-14 SSM/I as backup sensors. In addition, the activation of radar calibration (RADCAL) beacons on DMSP F15 on August 14, 2006 seriously contaminates the 22.235 GHz channel. Without accurate measurements from this channel, water vapor related products cannot be correctly retrieved. Since it is desirable to take advantage of the closeness of scan times of F16 and F15 in order to compare SSMIS with SSM/I, data acquired from F15 before the activation of the RADCAL beacons will be used in our comparison study.

After preliminary analysis of the SSMIS TDRs distributed by Fleet Numerical Meteorology and Oceanography Center (FNMOC), it was found that the original TDRs display notable anomalies, compared to radiative transfer model outputs, and the scale of such anomalies also vary with frequency. For example, due to the solar heating of reflector when spacecraft emerging from earth or spacecraft shadow and warm load solar intrusions, the lower atmosphere sounding (LAS) temperature channels may have biases reaching a peak about 2 K (Kunkee et al. 2008; Wessel et al. 2008; Swadley et al. to be submitted). In fact, reflector emission occurs for all scenes where the reflector and scene temperature differ, but its impact is most notable when reflector emerges from shadow and solar elevation angles are impinging from below the canister top, resulting in a dramatic jump in the reflector face temperature of 70 K or more. In our study, Earth and spacecraft shadowing only occur on the ascending portion of the rev in the December 2005 to February 2006 time frame. Nevertheless, SSM/I-like channels, especially those below 40 GHz, which are primarily used to produce environmental parameters in our study, do not exhibit very significant anomalies as LAS, UAS and Moisture sensing channels do. However, due to the apparent frequency dependence in the main reflector emissivity, there are residual biases that affect the 91.655 GHz in a more significant manner. The biases could in turn cause residual error in the EDRs. Because of the poor surface emissivity information forward model cannot well simulate the radiance at 91.655 GHz. But,

with the data sets matched using Simultaneous Conical Overpassing (SCO) and comparisons between F16 and F15 over global areas, the difference of mean TDR bias of the imaging channels between F16 and F15 between high latitudes and cloud free areas is found to be 0.5 K or less except for 91.655 GHz channels (Yan and Weng 2008), in which the biases come from both frequency shifting from 85.5 GHz in F15 and the difference in emission and scattering from atmosphere. At the same time, the resulting 'bias' in F16 TDRs, SDRs and EDRs are also dependent on the temperature difference between the main reflector surface and the scene temperature, which complicates the assessment. The assessment is further complicated by the slight frequency difference between F15 (85.5 GHz) and F16 (91.655 GHz).

The TDR data actually contains earth-located sets of antenna temperature. In the retrieval of parameters, not only antenna temperature but also brightness temperature will be used. The brightness temperature (Sensor Data Record or SDR) is obtained after Doppler correction, cross polarization and spill-over correction (or antenna pattern correction) on TDR data. In our retrieval, a set of coefficients was provided by Navy Research Lab (NRL) and is applied to linearly map the SSMI/S imaging channels from TDR to SDR. The coefficients are based on collocated F16 SSMI/S and F15 SSM/I imaging channel data. Note that that this linear mapping also converts SSMI/S 91.655 GHz to 85.5 GHz.

At both NRL and NOAA/NESDIS, algorithms are proposed to effectively detect and correct TDR anomalies caused by different factors. In these recalibration algorithms (Kunkee et al. 2008; Wessel et al. 2008; Swadley et al. to be submitted), the effect of solar radiation contamination on warm loads which affects TDRs in LAS channels, is dynamically detected through a Fast Fourier Transform (FFT) analysis. The regular periodic bias components identified by FFT are then removed. Research (Yan and Weng 2008) showed that nonlinearity terms in calibration equation could contribute to imaging channels TDR bias, therefore a set of nonlinear calibration coefficients are also derived to reduce the bias.

The TDRs actually contain earth-located sets of brightness temperature directly converted from the original sensor counts. However, due to the sensor hardware limitation or deficiency, e.g. feedhorn spillover loss and unavoidable leak of vertical polarization signal into horizontal polarization receiver, the antenna pattern correction (APC) is needed to correct such errors in order to obtain usable sensor brightness temperature (a.k.a Sensor Data Records or SDRs). In our study, the APC algorithm consists of a linear correction for the feedhorn spillover loss and cross-polarization coupling as shown in Eq. (1).

$$TB_{v(h)} = \frac{[TA_{v(h)} - a_{v(h)} TA_{h(v)}]}{\eta_{v(h)}(1 - a_{v(h)})} \qquad (1)$$

Where,

$TB_{v(h)}$ = SDR at vertical (horizontal) polarization

$TA_{v(h)}$ = TDR at vertical (horizontal) polarization

$\eta_{v(h)}$ = Feedhorn spillover factor

$a_{v(h)}$ = Cross-polarized coupling coefficient

Because the maximum cross-polarization occurs when the SSMIS views a cloudless dry atmosphere over calm ocean surface, $a_{v(h)}$ approaches zero in LAS and UAS channels. Only the spillover correction term is kept in the APC linear equation for those channels. The DMSP

F16 SSMIS has a larger than expected correction for antenna cross polarization effects even though the APC for SSMIS was originally intended to correct primarily for antenna spillover. In our study, the DMSP F16 SSMIS SSM/I-like lower frequency channels' linear mapping coefficients and APC are take from (Yan and Weng 2008) while linear mapping coefficients for 91.655 GHz channels were kindly provided by Mr. Steve Swadley of Naval Research Laboratory (NRL).

In this study, due to the different sampling resolution in SSM/I-like channels, we first produce global grid data at a resolution of 1/3 degree in latitude and longitude, and then separate them into two files corresponding to ascending and descending nodes. Next, a set of empirical linear remapping coefficients are applied to F16 SSM/I-like channels. Eq. (2) is used to make these channels signatures closer to corresponding heritage SSM/I channels.

$$TA'_{ichan} = \alpha_{ichan} + \beta_{ichan} TA_{ichan} \qquad (2)$$

Where,

TA'_{ichan} = remapped antenna brightness temperature

TA_{ichan} = original antenna brightness temperature

$\alpha_{ichan}, \beta_{ichan}$ = remapping coefficients

Note that such remapping also includes the mapping of F16 SSMIS 91.655 GHz to SSM/I 85.5 GHz so as to minimize the effects of the channel frequency shift, thereby allowing existing F15 SSM/I retrieval algorithms to be used with F16 data. Finally, the TDR to SDR conversion will be implemented by applying the linear APC algorithm to the remapped TDRs, as shown in Eq. (1).

The retrieval algorithms used to generate environmental products were previously developed by the SSM/I Cal/Val science team and have been widely used at NOAA since 1990s, as described in (Ferraro et al. 1996). The products used in this evaluation include total precipitable water (TPW), cloud liquid water path (LWP), snow and sea ice coverage, land surface temperature (LST), rainfall rate, and land emissivity as shown in Table 1.

TABLE 1: Summary of Heritage Retrieval Algorithms

Parameter	Channels	Units	Area	Reference
Total Precipitable Water	19.35V, 22.235V, 37.0V	mm	Ocean	(Alishouse et al. 1990)
Cloud Liquid Water	19.35V, 22.235V, 37.0V, 85.5H	mm	Land	(Weng and Grody 1994; Weng et al. 1997)
Snow Cover	19.35V/H, 22.235V, 37.0V, 85.5V		Land	(Grody 1991; Grody and Basist 1996)
Sea Ice Cover	19.35V/H, 22.235V, 37.0V/H, 85.5V		Ocean	unpublished
Land Surface Temperature	22.235V, 37.0V, 85.5V	K	Land	(Weng and Grody 1998)
Rain Rate	19.35V, 22.235V, 37.0V, 85.5V	mm/hr	All	(Grody 1991; Ferraro and Marks 1995)
Land Emissivity	19.35V/H, 22.235V, 37.0V/H, 85.5V/H		Land	(Weng et al. 2001; Yan and Weng 2003)

In addition to comparing the global imaging of retrieval figures, we also plot them as scatter diagrams for TPW, LWP, land surface temperature, and land emissivity retrievals in order to give readers more straightforward sense of whether heritage retrieval algorithms are fit for the

application to F16 SSM/I-like channels, and whether the F16 SSMIS TDR recalibration algorithm performs well.

Results and Discussion

To demonstrate the product retrieval quality and stability, data between December 2005 and February 2006 (DJF) are processed. By evaluating these products from hydrometeor (TPW, LWP and RR) to land surface products (LST, emissivity) as well as snow and ice cover, we may not only better understand the quality of DMSP F16 SSMIS but also keep the continuity of heritage environmental product algorithms retrieved from preexisting sensors in DMSP. In this section, each product will be illustrated and statistical analyses on several products will also be given.

Total Precipitable Water

The water vapor path retrieval, also known as total precipitable water (TPW), has been made over ocean from passive microwave instruments since 1987 when the first SSM/I was launched on board DMSP F-8 satellite. The algorithm was updated from (Alishouse et al. 1990) by using brightness temperatures at 19.35V, 22.235V, 37.0V, and 85.5V. As one of the most accurate parameters retrieved by passive microwave sensors, the error is only around 10% on a globally averaged basis compared with radiosondes observations. In our study, a slight modification is applied to Alishouse et al.'s original algorithm in order to obtain more accurate results under extreme weather conditions.

$$\begin{aligned} TPW &= 232.89 - 0.1486(TB_{19v}) - 0.3695(TB_{37v}) \\ &\quad - [1.8291 - 0.006193(TB_{22v})]TB_{22v} \end{aligned} \tag{3}$$

$$\begin{aligned} TPW_{corrected} &= -3.753 + 1.507(TPW) \\ &\quad - 0.1933(TPW)^2 + 0.00219(TPW)^3 \end{aligned} \tag{4}$$

In the retrieval process, TPW is firstly calculated using Eq. (3). At the same time, a scattering index is also computed (the detail of this index will be introduced in the discussion of rain rate retrieval). Whenever the scattering index is greater than 10K, the additional cubic correction is made to the original TPW as shown in Eq. (4).

Plotted in Fig. 1(a) and (b) are the TPW retrieved from F16 and F15, respectively. Please note that no TPW is retrieved over sea ice due to its high and variable emissivity. From both figures, we can observe many similar features and phenomena associated with the Inter-tropical Convergence Zone (ITCZ), South Pacific Convergence Zone (SPCZ) and South Atlantic Convergence Zone (SACZ). Fig. 5(a) is a statistical comparison between TPW retrievals from F16 and F15. The mean bias, standard deviation (STDEV) and root mean square (RMS) are given in Table 3. It seems that the preprocessing of F16 SSMIS data produces a good quality of the TPW from its imager channels at 19.35 GHz, 22.235 GHz and 37.0 GHz.

Cloud Liquid Water Path

The retrieval algorithm for cloud liquid water path (LWP), adopted in our study, was introduced in (Weng and Grody 1994; Weng et al. 1997). This algorithm makes use of brightness temperature measurements at both low and high frequencies to retrieve LWP in precipitating and non-precipitating clouds over ocean. Three LWPs are pre-calculated using three different channel combinations (19.35 V/22.235 V, 37.0V/22.235 V, and 85.5 H/22.235 V). The final LWP is determined by several criteria, as shown in Eq. (5). Fig. 3 and Fig. 4 give

the rain rate retrieval from F15 and F16. Again, we found quite similar distribution pattern of rainfall rate all over the world in both figures. Most global critical weather regions are emphasized, such as ITCZ. The rain rate distribution over ocean is also well corresponding to the cloud liquid water distribution in previous section.

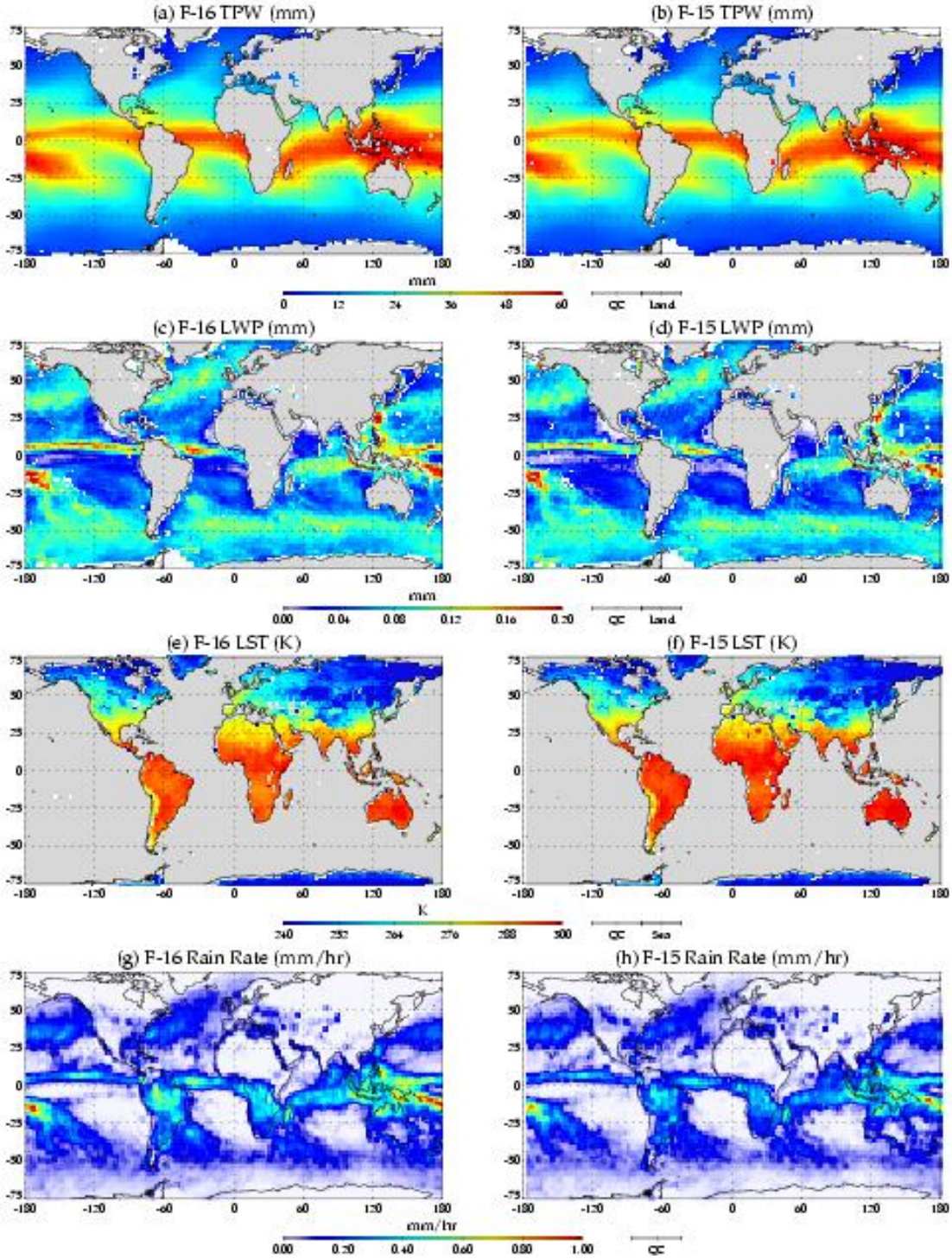

Fig. 1. TPW, LWP, LST and RR retrieved from F16 SSMIS and F15 SSM/I

$$LWP = \begin{cases} -3.20[\ln(290 - TB_{19v}) - 2.8 - 0.42\ln(290 - TB_{22v})], & LWP > 0.7 \\ -0.44[\ln(290 - TB_{85h}) - 1.6 + 1.35\ln(290 - TB_{22v})], & LWP > 0.28 \; and \; TPW < 30 \\ -1.66[\ln(290 - TB_{37v}) + 2.9 + 0.35\ln(290 - TB_{22v})], & else \end{cases} \quad (5)$$

This algorithm improves the former LWP retrievals by detecting LWP both in optically thin stratus and low-level clouds as well as highly convective clouds. The global LWP retrievals in boreal winter using F15 and F16 data are given in Fig. 1(c) and (d).

Cloud liquid water path retrieved from the two sensors are similar in spatial distribution. Some expected features have been captured in the global figures, such as strong convection over western Pacific warm pool, SPCZ and SACZ. However, along continental coast and sea ice edges there are some anomalously large LWP points. This may be caused by a mismatch of TDRs or contamination of surface sea ice. Meanwhile, near the high LWP areas, some anomalously low points may be due to the saturation of SSMIS imaging channels from heavy precipitation. The correlation between F15 and F16 is presented in Fig. 5(b) and is nearly linear. The increased scatter at higher LWP is probably due to the mismatch of observations and spatial inhomogeneity of clouds and precipitation. However, the small mean bias and STDEV indicate that the LWP retrieval from SSMIS is reliable and can be used for operation.

Land Surface Temperature

The land surface temperature (LST) algorithm for SSM/I was originally presented in (Weng and Grody 1998). As a linear regression algorithm developed from ground truth data, LST can be easily obtained over crop/range, moist and dry soils and other surface types. SDR measurements at 22.235 GHz V, 37.0 GHz V and 85.5 GHz V are used in this algorithm as shown by Eq. (6).

$$\begin{aligned} LST = \; & 0.02509[1.7167 - 0.005514(TB_{22v})]TB_{22v} \\ & -[0.1083 + 0.001976(TB_{37v})]TB_{37v} \\ & +[1.1763 - 0.000636(TB_{85v})]TB_{85v} \end{aligned} \qquad (6)$$

The global retrieval results can be found in Fig. 1(e) and (f). The LST patterns of F15 and F16 are highly consistent with each other. Compared to the summer season retrievals (not shown here) which shows the expected changes, most of Eurasia presents a lower LST due to the snow cover. However, it is shown (see Fig. 5(c)) that the mean LST of F15 is about 1.5 K higher than that of F16. The bias and standard deviation also increase with increasing LST. The outliers with large bias in Fig.5(c) are probably caused by measurement mismatch along coastal regions and the deficiency in the remapping algorithm which excludes scattering and emission adjustment. Overall, the SSM/I LST retrieval algorithm may be migrated to SSMIS for operational use but there is still a need to refine the remapping coefficients that convert SSMIS brightness temperatures at 91.655 GHz to SSM/I brightness temperature at 85.5 GHz, since Eq. (6) are used for both SSM/I and SSMIS.

Rain Rate

The rainfall rate (RR) algorithm developed at NESDIS (Ferraro and Marks 1995) makes use of the scattering of upwelling radiation by precipitation-size ice particles and large raindrops at 85 GHz to detect rainfall both over land and oceans. The difference between actual and an estimated (through 19.35 GHz V and 22.235 GHz V observation) brightness temperature at 85.5 GHz V, called ”scattering index” in (Grody 1991), is calculated by Eq.(7).

$$SI = EST_{TB_{85v}} - TB_{85v} \qquad (7)$$

Where,

$$EST_{TB_{85v}} = \begin{cases} 438.5 - 0.46(TB_{19v}) - 1.735(TB_{22v}) + 0.00589(TB_{22v})^2, & land \\ -182.7 - 0.75(TB_{19v}) + 2.543(TB_{22v}) - 0.00543(TB_{22v})^2, & ocean \end{cases}$$

A rain indicator is obtained if SI is greater than 10K. In addition, the LWP retrieval is also used over ocean to identify the rainfall area. As a result, the minimum detectable rain rate is about 0.5 mm/h over land and 0.2 mm/hr over ocean. Fig. 1(g) and (h) display the rain rate retrieval from F16 and F15. Over ocean, RR retrievals from each sensor correlate highly to their own high LWP retrieval regions and also between each other. One can also easily find heavy rainfall over critical areas, such as the western Pacific warm pool and SPCZ. The smooth continuous RR transition between land and ocean in both figures confirms that the RR retrieval algorithm can correctly catch rainfall signals both over land and over ocean. However, even though geophysical locations for RR are close to each other over land, the scales are not consistent between F15 and F16. As RR is a parameter highly dependent on the scan time, bias could be very large even when the scan time difference between F15 and F16 is around 30 minutes. Therefore, it is yet to be determined whether the source of bias is due to scan time difference or sensor differences. Furthermore, because the RR retrieval also uses 85.5 GHz channel measurements remapped from 91.655 GHz in F16 SSMIS by globally derived linear coefficients, the more localized RR retrieval will present a larger bias between F16 SSMIS and F15 SSM/I.

Sea Ice

Several sea ice concentration and ice age algorithms have been developed for passive microwave radiometers (Rubinstein et al. 1994; Markus and Cavalieri 2000). Comparison between these algorithms has also been performed (Markus and Dokken 2002; Shokr and Markus 2006). To keep the continuity of our heritage study of sea ice cover, a simple algorithm is used to identify the presence of sea ice. The retrieval function is given as,

$$\begin{aligned} ICE = \; & 91.9 - 2.99(TB_{22v}) + 2.85(TB_{19v}) \\ & - 0.39(TB_{37v}) + 0.50(TB_{85v}) \\ & + 1.01(TB_{19h}) - 0.90(TB_{37h}) \end{aligned} \qquad (8)$$

where ICE greater than 70% is defined as sea ice. In our sea ice averaging processing, the percentage of sea ice present during the three winter months (December, January, February) is calculated. Fig. 2(a), (b), (c), and (d) give the sea ice cover retrieved from F16 and F15, respectively. The sea ice

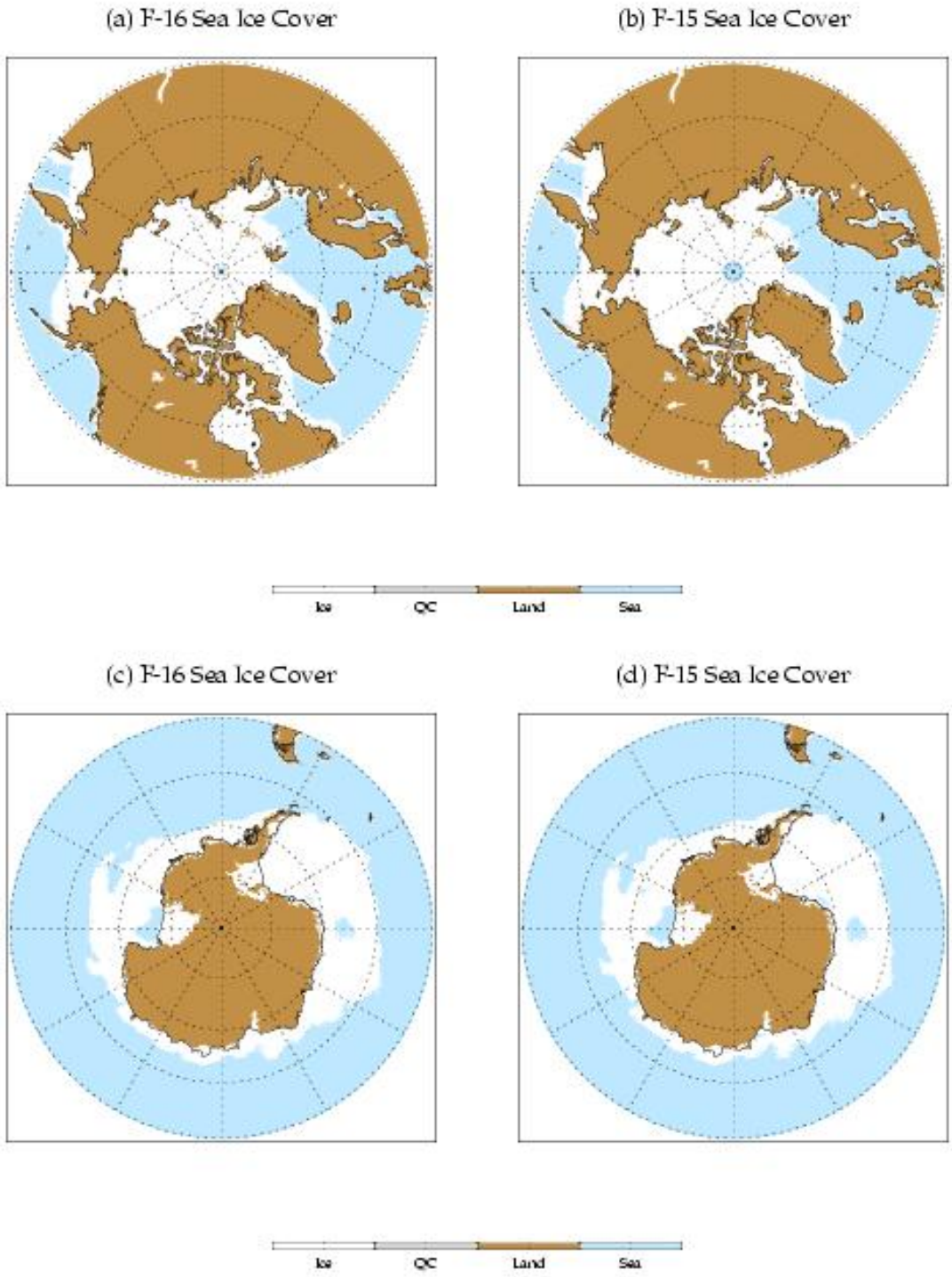

Fig 2. Sea Ice Cover retrieved from F16 SSMIS and F15 SSMI near North and South Pole

cover in the northern hemisphere extends south exceeding 50oN both along east coast of North America and the Eurasian continent. Due to the North-Atlantic current, there is a lack of sea ice in the Barents Sea. Overall, the sea ice cover of F15 SSM/I and F16 SSMIS are in good agreement.

Snow Cover

The snow coverage retrieval algorithm used in our study was published in (Grody 1991; Grody and Basist 1996). It includes measurements at 85.5 GHz to detect shallow snow cover and also screens for precipitation, cold desert, frozen ground, and other signatures which could potentially increase retrieval error. In this algorithm, brightness temperature measurements at 19.35 GHz V, 22.235 GHz V, 37.0 GHz V and 85.5 GHz V are used.

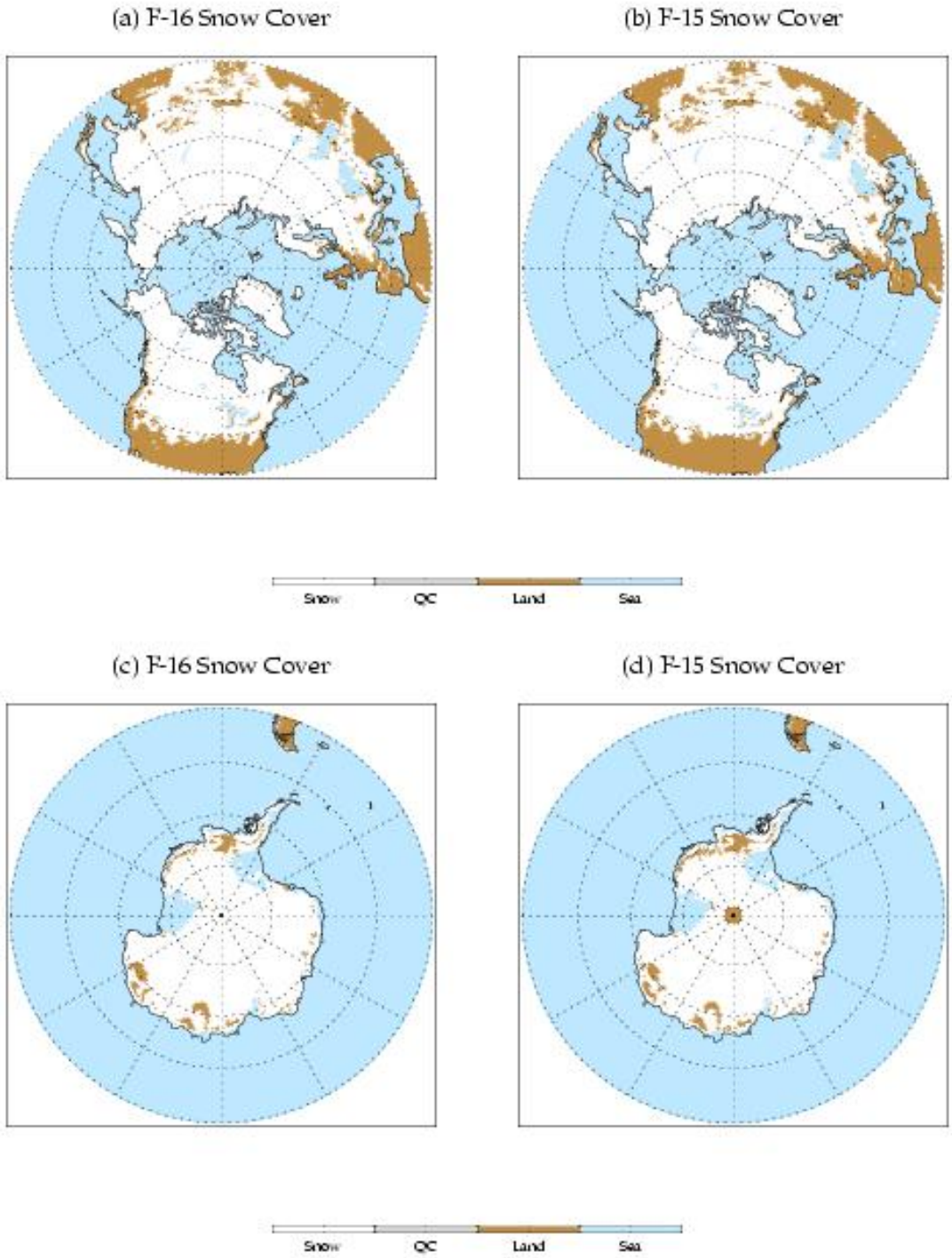

Fig 3. Snow Cover retrieved from F16 SSMIS and F15 SSM/I near North and South Pole

Snow cover retrieved from F15 and F16 in the northern hemisphere and the Antarctic are shown in Fig.3(a), (b), (c), and (d). Because the retrievals are from December 2005 to February

2006, most of areas north of 40oN are covered by snow. Overall, the snow cover retrievals from two sensors are highly consistent. However, because snow retrieval also uses 85.5 GHz measurements to derive the scattering parameter, the globally derived remapping coefficient may also affect snow cover retrieval. Therefore stratified remapping coefficients will be developed.

Land Emissivity

The land emissivity is an important parameter that can be used to infer some other geophysical parameters, such as soil moisture, vegetation water and soil wetness. The land emissivity algorithm was published in (Weng et al. 2001; Yan and Weng 2003). For low frequency channels at 19.35 GHz V/H and 37.0 GHz V/H, their emissivity is based on a linear regression relationship among all seven SSM/I-like channel SDR measurements, shown in Eq. (9).

$$\begin{aligned}\varepsilon = \; & a_0 + a_1(TB_{19v}) + a_2(TB_{19h}) + a_3(TB_{22v}) \\ & a_4(TB_{37v}) + a_5(TB_{37h}) + a_6(TB_{85v}) + a_7(TB_{85h})\end{aligned} \tag{9}$$

For emissivity at 85v and 85h, a nonlinear relation is built from 37.0 GHz V and 85.5 GHz V/H by Eq. (10),

$$\begin{aligned}\varepsilon = \; & b_0 + [b_1 + b_2(TB_{37v})](TB_{37v}) \\ & [b_3 + b_4(TB_{85v})](TB_{85v}) + [b_5 + b_6(TB_{85h})](TB_{85h})\end{aligned} \tag{10}$$

Table 2 presents the coefficients of in Eq. (9) and Eq. (10) for each channel. Here we choose

TABLE 2: Coefficients Used in Land Emissivity Retrieval

Channel	a0	a1	a2	a3	a4	a5	a6	a7
19.35 V	0.5098	4.4664E-3	-6.0427E-6	-2.5285E-3	-2.3725E-3	9.8163E-4	-2.2269E-3	-1.3193E-3
19.35 H	0.4290	1.0685E-3	4.0082E-3	-2.9672E-3	1.4281E-3	1.7393E-3	-1.0247E-3	-2.2088E-3
22.235 V	0.5098	4.4664E-3	-6.0427E-6	-2.5285E-3	-2.3725E-3	9.8163E-4	-2.2269E-3	-1.3193E-3
37.0 V	0.3186	-1.5225E-3	1.7213E-3	-3.7164E-4	6.5607E-3	8.1213E-4	-1.7678E-3	-1.7250E-3
37.0 H	0.2622	-1.5095E-3	-1.9587E-5	5.0142E-4	6.8795E-4	5.7910E-3	-7.1539E-4	-2.1267E-3
Channel	b0	b1	b2	b3	b4	b5	b6	
85.5 V	-0.9435	4.1137E-3	-7.0109E-6	1.5677E-2	-3.1055E-5	-6.5089E-3	1.4984E-5	
85.5 H	-0.9788	3.0851E-3	-5.2696E-6	7.4612E-3	-2.2772E-5	2.9755E-3	4.5324E-6	

retrievals at 19.35 GHz (H/V) and 37.0 GHz (H/V) for demonstration purpose. The results are shown in Fig. 4. Because the channel frequency shifts from 85.5 GHz in F15 SSM/I to 91.655 GHz in F16 SSMIS, we do not include these two channel emissivities in this comparison.

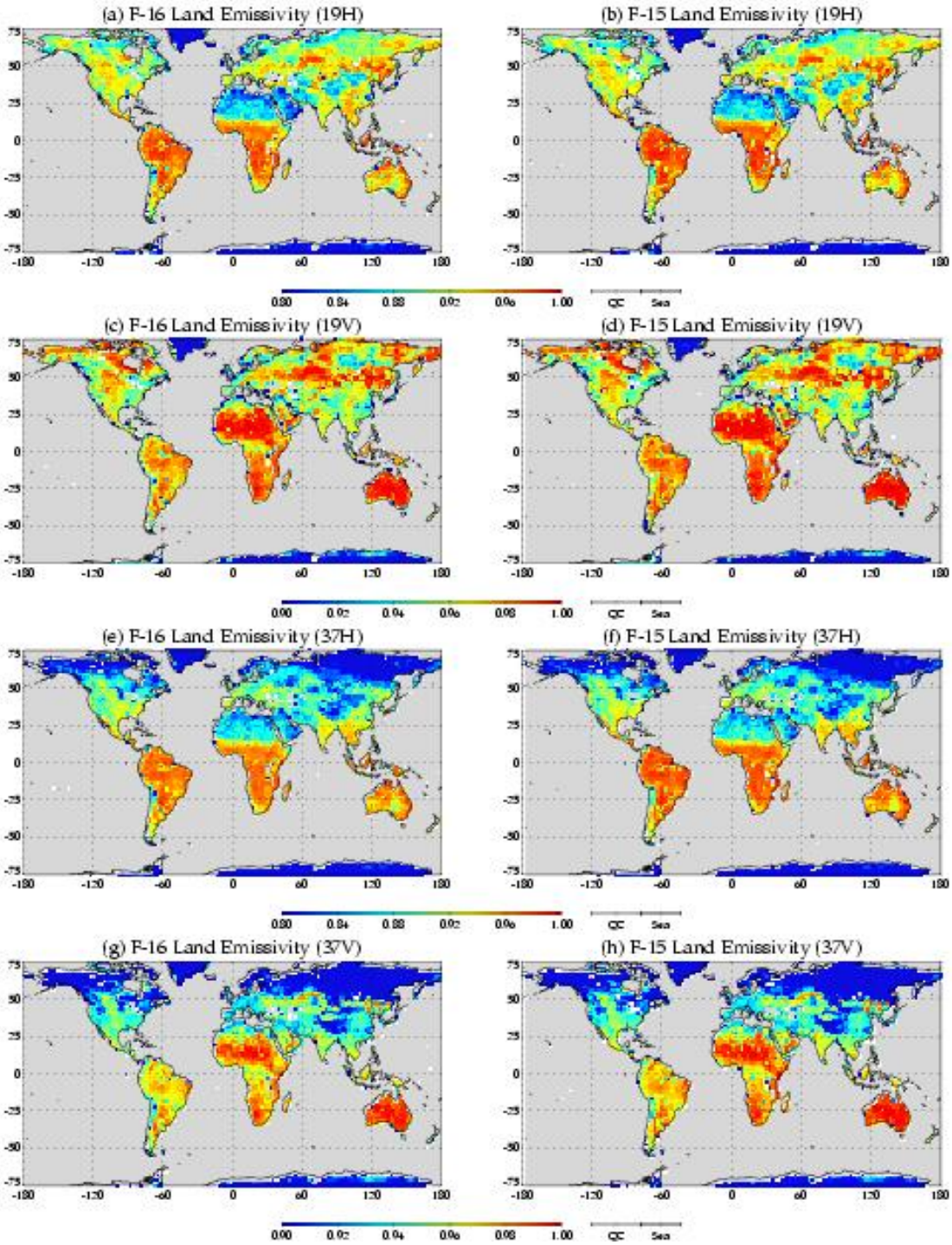

Fig 4. Land Emissivity retrieved from F16 SSMIS and F15 SSM/I at 19.65 V/H and 37.5 V/H

The retrievals from each sensor capture land surface signatures well. For example, vertical polarization over deserts shows a larger emissivity compared to horizontal polarization. In addition, emissivity retrieved from 37.0 GHz is more sensitive to snow surface condition than 19.35 GHz channels. Generally speaking, the retrievals are very well correlated. However, very similar to the land surface temperature retrieval, the difference between emissivities retrieved for F16 and F15 at 37.0 GHz horizontal polarization is observed over a large dynamic range as

the emissivity increases (Fig. 5(d)). Furthermore, the differences become larger in the desert and snow cover areas where surface scattering is present.

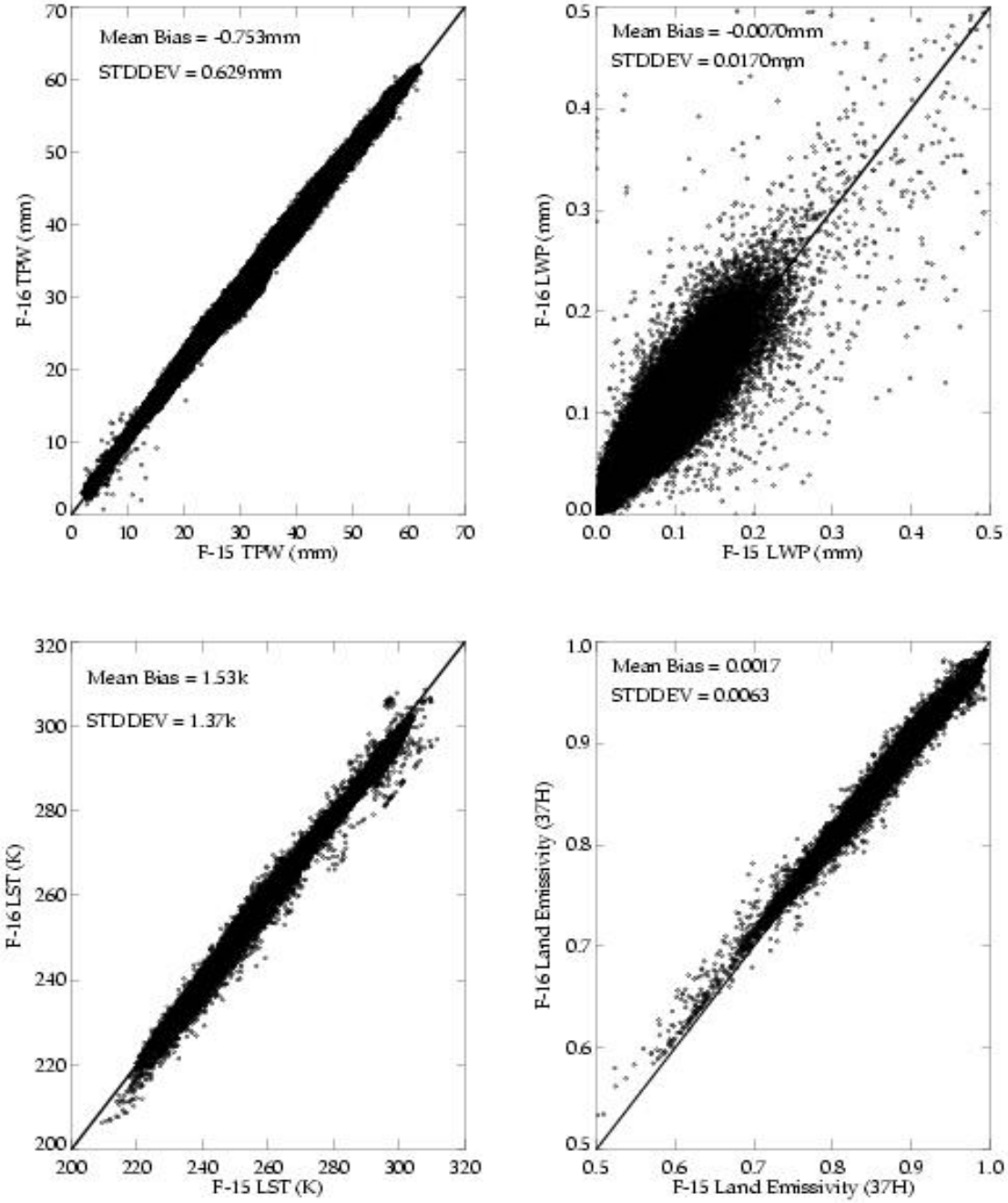

Fig 5. Scatter plot of TPW, LWP, LST and emissivity at 37.0H from DMSP F15 SSMI and DMSP F16 SSMIS Imaging Channels

Summary

Retrievals of hydrological and surface parameters from F16 SSMIS are demonstrated using the SSM/I algorithms. The products are compared for three months of data from both sensors. All F16 TDRs have been reprocessed as the experimental TDR data. The procedure for TDR to SDR correction and the remapping of F16 SSMIS imaging channels to F15 SSM/I is based on

the algorithm from NRL. After the reprocessing on F16 SSMIS, contamination of measured antenna temperatures, direct solar radiation, cross polarization coupling, and antenna spillover are effectively reduced. The F16 SSMIS to SSM/I imaging channel remapping is a critical step in our study because it allows us to use the same algorithms for two instruments.

Both satellites' orbit data have been processed to 1/3 degree grid data. Because the time difference between DMSP F15 and F16 is about 30 minutes, most retrieval products will not be affected much by such small time variation except for rain rate, which is temporally variable. The products, including TPW, LWP, LST, Snow Cover, Sea Ice Cover, and land emissivity, are presented. It is shown that the retrievals from both sensors demonstrate a high level of agreement with each other. The statistical results based on the seasonal averaged data for TPW, LWP, LST, RR and emissivity at five SSM/I channels are listed in Table 3. Both the relatively small mean bias and

TABLE 3: Statistical Analyses on Retrieval Bias of Selected Parameters

Parameter	Mean Bias	STDEV	RMS
TPW	-0.753 mm	0.629 mm	0.981 mm
LWP	-0.007 mm	0.017 mm	0.018 mm
LST	1.531 K	1.373 K	2.056 K
RR	-0.013 mm/hr	0.110 mm/hr	0.111 mm/hr
$\varepsilon_{19.35V}$	0.0017	0.0034	0.0038
$\varepsilon_{19.35H}$	0.0019	0.0045	0.0049
$\varepsilon_{22.235V}$	0.0017	0.0034	0.0038
$\varepsilon_{37.0V}$	0.0007	0.0050	0.0051
$\varepsilon_{37.0H}$	0.0017	0.0063	0.0065

standard deviation prove that F16 SSMIS data can be successfully using the retrievals previously developed for use with SSM/I channels. However, retrievals sensitive to 85.5 GHz measurements, such as the land surface temperature and the land emissivity, displays some biases. For example, over Sahara deserts LST retrieved from F16 is slightly lower than that from F15 while no significant biases over non-desert areas. Because LST retrieval algorithm uses the quadratic term of vertically polarized 85.5 GHz brightness temperature, the higher scattering feature of 91.655 GHz in F16, which even has been remapped to 85.5 GHz, might be the source of the biases. Therefore, the F16 SSMIS to SSM/I remapping algorithm requires further improvement over the simple linear remapping algorithm used to correct the change from 85.5 to 91.655 GHz which cannot account for scattering and emission effects under all weather and surface conditions.

Among these evaluated retrieval algorithms, other issues are also notable. For example, rain rate retrievals along coastal regions or sea ice boundaries always give some non-zero values. This may be due to the mixing of land and ocean or sea ice within a single footprint while using an emission-based algorithm. Fortunately, because DMSP F16 SSMIS contains not only imaging channels but environmental channels at 150 GHz and 183.31 GHz, new algorithms based on particle scattering are being developed for precipitation applications (Weng and Grody 2000; Zhao and Weng 2002). This will allow rain rate to be inferred by using the direct relation to cloud ice water path (IWP). Meanwhile, the IWP retrieval will directly use channel measurements at 91.655 GHz. Thus, there is no need for remapping F16 SSMIS and SSM/I for precipitation studies.

Acknowledgment

The authors would like to thank TGARS Guest Editor, Dr. David Kunkee, Aerospace Corporation, and two anonymous reviewers for their thorough reviews and recommendations to improve our manuscript as well as overall studies. We would also like to acknowledge Mr. Steve Swadley of NRL for providing DMSP F16 SSM/I-like channel remapping and TDR to SDR conversion coefficients in making this study possible. The authors are also grateful to Drs. Banghua Yan, Sid-Ahmed Boukabara and Kevin Garrett for providing constructive suggestions in writing this paper.

Disclaimer

The contents of this study are solely the opinions of the authors and do not constitute a statement of policy, decision, or position on behalf of NOAA or the U.S. Government.

References

Alishouse, J. C., S. A. Snyder, J. Vongsathorn, and R. R. Ferraro, 1990: Determination of Oceanic Total Precipitable Water from the SSM/I. *IEEE Trans. Geosci. Remote Sens.*, **28,** 811-816.

Deblonde, G., 1999: Variational assimilation of SSM/I total precipitable water retrievals in the CMC analysis system. *Monthly Weather Review*, **127,** 1458-1476.

Ferraro, R. R. and G. F. Marks, 1995: The Development of SSM/I Rain-Rate Retrieval Algorithms Using Ground-Based Radar Measurements. *Journal of Atmospheric and Oceanic Technology*, **12,** 755-770.

Ferraro, R. R., F. Weng, N. C. Grody, and A. Basist, 1996: An eight-year (1987-1994) time series of rainfall, clouds, water vapor, snow cover, and sea ice derived from SSM/I measurements. *Bulletin of the American Meteorological Society*, **77,** 891-905.

Grody, N. C., 1991: Classification of Snow Cover and Precipitation Using the Special Sensor Microwave Imager. *Journal of Geophysical Research-Atmospheres*, **96,** 7423-7435.

Grody, N. C. and A. N. Basist, 1996: Global identification of snowcover using SSM/I measurements. *IEEE Trans. Geosci. Remote Sens.*, **34,** 237-249.

Hou, A. Y., D. V. Ledvina, A. M. da Silva, S. Q. Zhang, J. Joiner, R. M. Atlas, G. J. Huffman, and C. D. Kummerow, 2000: Assimilation of SSM/I-derived surface rainfall and total precipitable water for improving the GEOS analysis for climate studies. *Monthly Weather Review*, **128,** 509-537.

Kunkee, D. B., S. D. Swadley, G. A. Poe, Y. Hong, and M. F. Werner, 2008: Special Sensor Microwave Imager Sounder (SSMIS) Radiometric Calibration Anomalies—Part I: Identification and Characterization. *IEEE Trans. Geosci. Remote Sens.*, **46,** 1017-1033.

Markus, T. and D. J. Cavalieri, 2000: An enhancement of the NASA Team sea ice algorithm. *IEEE Trans. Geosci. Remote Sens.*, **38,** 1387-1398.

Markus, T. and S. T. Dokken, 2002: Evaluation of late summer passive microwave Arctic sea ice retrievals. *IEEE Trans. Geosci. Remote Sens.*, **40,** 348-356.

Okamoto, K. and J. C. Derber, 2006: Assimilation of SSM/I radiances in the NCEP global data assimilation system. *Monthly Weather Review*, **134,** 2612-2631.

Rubinstein, I. G., D. M. Nazarenko, and S. Tam, 1994: Passive microwave systems. *Remote Sensing of Sea Ice and Icebergs***,** 177-257.

Shokr, M. and T. Markus, 2006: Comparison of NASA Team2 and AES-York ice concentration algorithms against operational ice charts from the Canadian ice service. *IEEE Trans. Geosci. Remote Sens.*, **44,** 2164-2175.

Swadley, S., G. Poe, D. Kunkee, W. Bell, and Y. Hong, to be submitted: Special Sensor Microwave Imager Sounder (SSMIS) radiometric calibration anomalies—Part II:

Anomaly descriptions and mitigation strategies for radiance assimilation. *IEEE Trans. Geosci. Remote Sens.*

Tsuyuki, T., 1997: Variational data assimilation in the tropics using precipitation data .3. Assimilation of SSM/I precipitation rates. *Monthly Weather Review*, **125,** 1447-1464.

Weng, F. and N. C. Grody, 1994: Retrieval of Cloud Liquid Water Using the Special Sensor Microwave Imager (SSM/I). *Journal of Geophysical Research-Atmospheres*, **99,** 25535-25551.

——, 1998: Physical retrieval of land surface temperature using the special sensor microwave imager. *Journal of Geophysical Research-Atmospheres*, **103,** 8839-8848.

——, 2000: Retrieval of ice cloud parameters using a microwave imaging radiometer. *Journal of the Atmospheric Sciences*, **57,** 1069-1081.

Weng, F., B. Yan, and N. C. Grody, 2001: A microwave land emissivity model. *Journal of Geophysical Research-Atmospheres*, **106,** 20115-20123.

Weng, F., N. C. Grody, R. Ferraro, A. Basist, and D. Forsyth, 1997: Cloud liquid water climatology from the special sensor microwave/imager. *Journal of Climate*, **10,** 1086-1098.

Wessel, J., R. W. Farley, A. Fote, Y. Hong, G. A. Poe, S. D. Swadley, B. Thomas, and D. J. Boucher, 2008: Calibration and Validation of DMSP SSMIS Lower Atmospheric Sounding Channels. *IEEE Trans. Geosci. Remote Sens.*, **46,** 946-961.

Yan, B. and F. Weng, 2003: Ten-year (1993-2002) time-series of microwave land emissivity. *Microwave Remote Sensing of the Atmosphere and Environment III. Edited by Kummerow, Christian D.; Jiang, JingShang; Uratuka, Seiho. Proceedings of the SPIE*, **4894,** 278-286.

——, 2008: Intercalibration Between Special Sensor Microwave Imager/Sounder and Special Sensor Microwave Imager. *IEEE Trans. Geosci. Remote Sens.*, **46,** 984-995.

Zhao, L. and F. Weng, 2002: Retrieval of ice cloud parameters using the advanced microwave sounding unit. *Journal of Applied Meteorology*, **41,** 384-395.